https://doi.org/10.55343/CogSust.109

Mathematical Model Derivation of Protean In-Wheel-Motor Used in EV Applications

Mahmoud Said Jneid
https://orcid.org/0000-0001-5407-285X
Department of Automotive Technologies, Budapest University of Technology and Economics, Budapest, Hungary
mah.jneid@edu.bme.hu

Peter Harth
https://orcid.org/0000-0003-4400-3986
Department of Automotive Technologies, Budapest University of Technology and Economics, Budapest, Hungary
harth.peter@kjk.bme.hu

Abstract

A Protean in-wheel-motor (IWM) is a special type of permanent magnet synchronous motor developed by Protean Electric for direct drive electric vehicle applications. The Protean IWM features a high fault-tolerance substantial for EV applications by dividing the stator into eight independent sub-motors. Each sub-motor features a balanced three-phase system with a spanning of 45°/360° mechanical/electrical on the stator periphery. In total, there are $8 \times 3 = 24$ phases on the stator distributed with a displacement between any two subsequent phases of 15°/120° mechanical/electrical. In this paper, the mathematical model of a Protean motor in a synchronous rotor frame *(d-q)* is derived based on a set of Park transforms corresponding to each sub-motor spatial and electrical distribution. The set of Park transforms is then adapted into one generalised Park transform that can be applied to any sub-motor by introducing an angle representing the beginning of each sub-motor.

Keywords

Protean, in-wheel-motor, sub-motor, fault-tolerance, mathematical model

1. Introduction

The rapid evolution of electric vehicles (EVs) has driven the demand for advanced motor technologies that offer high efficiency, reliability, and integration simplicity. In-wheel motors (IWMs) have become a groundbreaking technology for vehicle electrification, providing improved efficiency, reduced size, and greater design versatility compared to conventional onboard motors (Said Jneid et al., 2020). In addition, EVs that use IWMs as propulsion systems transport the traditional centralised vehicle motion control into allocated control through independent wheel torque control (Said Jneid, 2024). This does not only simplify the vehicle structure, but also takes the vehicle dynamic control integration to new levels where main elements (sensors, actuators) in the vehicle can be shared among different systems allowing for a holistic control with a reduced number of elements, smaller space, and lower costs (Said Jneid, 2024). The integration can happen not only on the hardware level but also on the vehicle system control level. For instance, IWMs actuators can be integrated with brake system actuators, namely electronic wedge brakes (EWBs) producing a pure brake-by-wire (BBW) system (Said Jneid and Joukhadar, 2019; Said Jneid, Zöldy and Harth, 2023). Brake actuator integration allows the blending of frictional and regenerative braking torques enabling functionalities of anti-lock braking system (ABS) based on an electronic version, namely regenerative anti-lock braking system (RABS) (Said Jneid and Harth, 2023a). On the vehicle control system level, IWMs allow the integration between different advanced chassis active-safety systems (ACAS) such as ABS and traction control system (TCS) (Said Jneid and Harth, 2023c), ABS, traction control systems (TCS), and torque vectoring (TV) (Said Jneid and Harth, 2023c, 2023b, 2023d). Several leading automotive and tyre manufacturers have introduced the conceptual designs of IWMs. Inspired by early conceptual IWMs, several companies have introduced advanced IWMs today, each distinguished by unique design, specifications, and target applications (Said Jneid, 2024). Permanent Magnet Synchronous

https://doi.org/10.55343/CogSust.109

Motors (PMSMs) are the ideal option for IWMs due to their high torque density, attributed to utilising Neodymium permanent magnets(Deepak et al., 2023; Feng et al., 2023). In terms of magnetic design, essential IWMs utilise radial flux configuration where the magnetic lines are aligned radially between the stator and the rotor across the air gap (Said Jneid, 2024). Recently, several companies have adopted axial flux topology for IWMs as they boast impressive power and torque densities strongly required for EV applications.

As a radial flux IWM, the Protean drive stands out as a cutting-edge solution designed to meet the unique challenges of EV applications(Hilton, 2016). Developed by Protean Electric, this innovative motor integrates the drive system directly into the wheels, eliminating the need for traditional drivetrains and significantly enhancing the overall vehicle design (Perovic, 2012; Fraser, 2018). The Protean IWM is a specialised permanent magnet synchronous motor (PMSM) engineered for direct-drive applications. Its design is notable for its high fault tolerance, a critical feature for ensuring reliability in EVs (Whitehead and Hilton, 2018). This is achieved by dividing the stator into eight independent sub-motors, each with a balanced three-phase system. These sub-motors are distributed around the stator periphery, with each one covering a 45° mechanical span or 360° electrical span (Perovic, 2012). This modular approach enhances fault tolerance, simplifies maintenance, and improves overall performance. A significant aspect of the Protean IWM's design is its ability to maintain performance even in the event of a failure in one or more sub-motors. This is crucial for the operational reliability of EVs, where motor failure can lead to significant downtime and safety concerns (Ifedi et al., 2012). The distributed nature of the sub-motors ensures that the motor can continue to operate, even with reduced performance, thereby providing a level of redundancy that is highly valued in automotive applications (Ifedi et al., 2011). In this paper, we delve into the mathematical modelling of the Protean IWM given in a synchronous rotor frame *(d-q)*.

To obtain the mathematical model for the Protean sub-motors, it is essential to first understand the motor winding configuration. In total, there are 24 phases distributed across eight sub-motors (8-sub-motor × 3-phase = 24). Each sub-motor occupies of 45° mechanical angle (mech.) on the stator periphery. The angle between two phases belonging to the same sub-motor is 15° mech. Phase A_1 of the sub-motor 1 starts at angle 0° mech., follows phase B_1 at 15°, and phase C_1 at angle 45°. Following, the sub-motor 2 A_2 phase begins at 45°, B_2 at 60°, and phase C_2 at 75°. This pattern repeats for the remaining six sub-motors. Figure 1 illustrates a schematic for the mechanical span and phase distributions of each Protean sub-motor along with the dedicated number of poles. Each sub-motor's phases are denoted by the letters A_n, B_n, and C_n, with '*n*' indicating the sub-motor number (*n*=1 to 8). The complete motor is designed with a 72/64 slots/poles configuration. Each phase of any sub-motor is distributed for three coils, resulting in a total of nine coils occupying nine slots on the stator. The number of poles corresponding to each sub-motor is eight, resulting in a mechanical angle reserved by each sub-motor of 45° as depicted in Figure 1 corresponding to an electrical angle of 360°. The electrical angle between the two phases is 15° × 8-Poles = 120°. Figure 2 presents a schematic diagram for sub-motor phase angle distributions in electrical degrees. Table 1 provides the mechanical and electrical span on the machine periphery with three-phase spatial and electrical angle distributions of each sub-motor.

https://doi.org/10.55343/CogSust.109

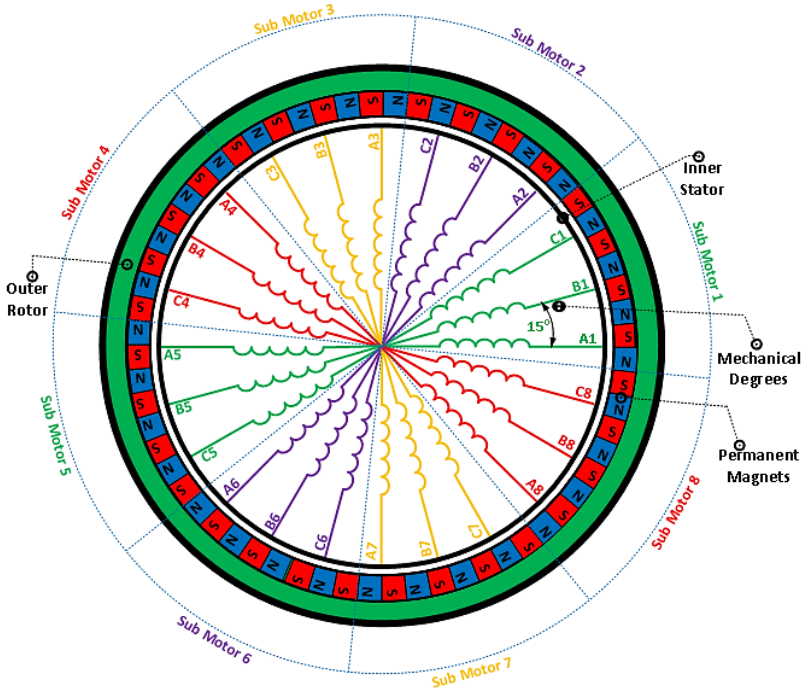

Figure 1. The mechanical span and phase angle distributions of each Protean sub-motor.

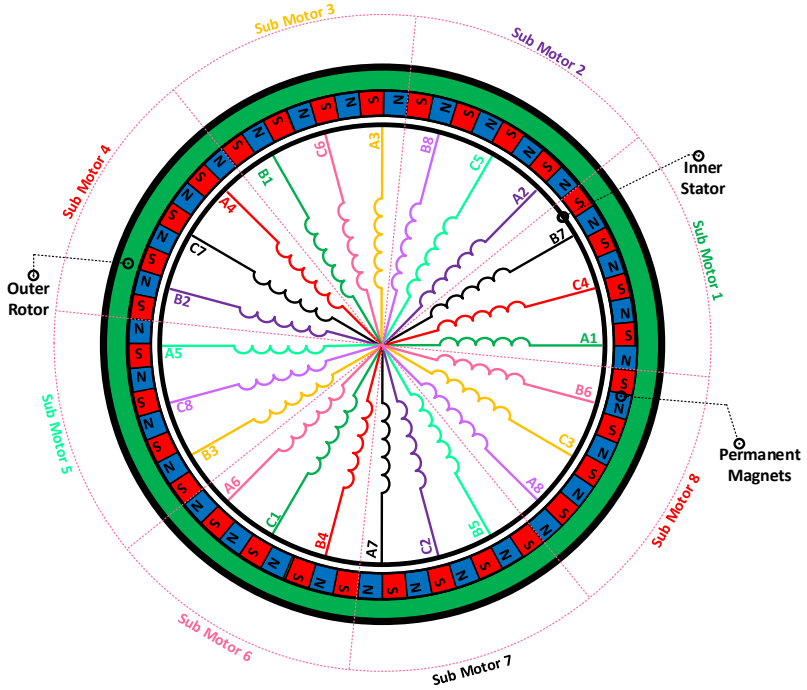

Figure 2. The electrical span and phase angle distributions of each of the Protean sub-motors.

https://doi.org/10.55343/CogSust.109

Table 1. The mechanical and electrical span on the machine periphery with a spatial and electrical three-phase distribution of each sub-motor.

Sub-motor No. (n)	Span Angle [Mech]	Span Angle [Elec]	Phase A Angle [Mech/ Elec]	Phase B Angle [Mech/ Elec]	Phase C Angle [Mech/ Elec]
1	0°–45°	360°	0° / 0°	15° / 120°	30° / 240°
2	45°–90°	360°	45° / 45°	60° / 165°	75° / 285°
3	90°–135°	360°	90° / 90°	105° / 210°	120° / 330°
4	135°–180°	360°	135° / 135°	150° / 255°	165° / 15°
5	180°–225°	360°	180° / 180°	195° / 300°	210° / 60°
6	225°–270°	360°	225° / 225°	240° / 345°	255° / 105°
7	270°–315°	360°	270° / 270°	285° / 30°	300° / 150°
8	315°–360°	360°	315° / 315°	330° / 75°	345° / 195°

2. Protean IWM Mathematical Model Given In The Stationary Reference Frame (A, B, C)

To obtain a simplified mathematical model for the Protean motor, the following considerations were imposed:

- Uniform air gap with constant width;
- Negligible magnetic leakage, as well as iron losses;
- Gaussian distribution of the magnetic field along the air gap;
- Perfect symmetry for the stator windings, i.e., equal resistances and inductances;
- Star point for each sub-motor is not connected;
- The mutual flux between the phase C_n of any sub-motor (n) and the phase A_{n+1} of the following sub-motor is neglected.

The voltage and flux for any balanced three-phase Protean sub-motor are given through the following equations:

$$u_{a_n} = R_s i_{a_n} + \frac{d\varphi_{a_n}}{dt} \quad (1)$$

$$u_{b_n} = R_s i_{b_n} + \frac{d\varphi_{b_n}}{dt} \quad (2)$$

$$u_{c_n} = R_s i_{c_n} + \frac{d\varphi_{c_n}}{dt} \quad (3)$$

$$\varphi_{a_n} = l_s i_{a_n} + M_s i_{b_n} + M_s i_{c_n} + \varphi_{fa_n} \quad (4)$$

$$\varphi_{b_n} = M_s i_{a_n} + l_s i_{b_n} + M_s i_{c_n} + \varphi_{fb_n} \quad (5)$$

$$\varphi_{c_n} = M_s i_{a_n} + M_s i_{b_n} + l_s i_{c_n} + \varphi_{fc_n} \quad (6)$$

where:

$u_{a_n}, u_{b_n}, u_{c_n}$: three-phase voltages of sub-motor *(n)*.

$i_{a_n}, i_{b_n}, i_{c_n}$: three-phase currents of sub-motor *(n)*.

$\varphi_{a_n}, \varphi_{b_n}, \varphi_{c_n}$: three-phase fluxes of sub-motor *(n)*.

$\varphi_{fa_n}, \varphi_{fb_n}, \varphi_{fc_n}$: three-phase flux linkages of each sub-motor *(n)*.

R_s, l_s, M_s: stator phase resistance, self-inductance, and mutual inductance of any sub-motor *(n)*, respectively.

The three-phase induced voltages are given as follows:

$$e_{a_n} = \varphi_{fa_n}\omega_r \cos(\theta_e - (n-1)\theta_{sm}) \quad (7)$$

$$e_{b_n} = \varphi_{fb_n}\omega_r \cos\left(\theta_e - \frac{2\pi}{3} - (n-1)\theta_{sm}\right) \quad (8)$$

$$e_{a_n} = \varphi_{fa_n}\omega_r \cos(\theta_e - \frac{4\pi}{3} - (n-1)\theta_{sm}) \quad (9)$$

Since all sub-motors' start points are not connected, the sum of the three-phase currents equals zero. Consequently, the equations for the voltages of the previous sub-motors can be rewritten as follows:

https://doi.org/10.55343/CogSust.109

$$L_s \frac{di_{a_n}}{dt} = u_{a_n} - R_s i_{a_n} + e_{a_n} \quad (10)$$

$$L_s \frac{di_{b_n}}{dt} = u_{b_n} - R_s i_{b_n} + e_{b_n} \quad (11)$$

$$L_s \frac{di_{c_n}}{dt} = u_{c_n} - R_s i_{c_n} + e_{c_n} \quad (12)$$

where:

$e_{a_n}, e_{b_n}, e_{c_n}$: the three-phase induced voltages of sub-motor *(n)*.

L_s: the stator phase transient inductance of any sub-motor *(n)*.

ω_r: mechanical rotor speed of Protean motor.

θ_e: rotor position in electrical degrees, equal $d\theta_e/dt = \omega_{re}$.

ω_{re}: electrical rotor speed of Protean motor, equal $\omega_{re}\ P\omega_r$.

P: rotor pole pairs of any sub-motor *(n)*.

θ_{sm}: angle between two same phases of subsequent sub-motors (e.g., A_1, A_2) equals 45°.

n: sub-motor number in the Protean motor, takes the range $n = 1\ to\ 8$.

The electromagnetic torque equation for any sub-motor *(n)* in the Protean motor is expressed in terms of the three-phase currents and electromagnetic forces according to the following:

$$T_{em_n} = \frac{1}{\omega_r}\left(e_{a_n} i_{a_n} + e_{b_n} i_{b_n} + e_{c_n} i_{c_n}\right) \quad (13)$$

The total torque of the Protean motor is the sum of all sub-motor torques, according to the following:

$$T_{em_n} = \frac{1}{\omega_r}\left(e_{a_n} i_{a_n} + e_{b_n} i_{b_n} + e_{c_n} i_{c_n}\right) \quad (14)$$

$$T_{em_{Eq}} = \sum_{n=1}^{8} T_{em_n} \mathrm{R} \quad (15)$$

The rotor mechanical speed is given as follows:

$$J_r \frac{d\omega_r}{dt} = T_{em_{Eq}} - T_L \quad (16)$$

With

$$T_L = (F_r + F_w + F_x)\omega_r \quad (17)$$

where:

J_r: the rotor moment of inertia, T_L: the motor's total load.

$T_{em_{Eq}}$: equivalent electromagnetic torque of Protean motor (all sub-motors),

F_r, F_w: friction coefficient of rotor and wheel, respectively.

F_x: wheel's longitudinal force.

Figure 3 illustrates the complete block diagram of Protean sub-motors in a stationary reference frame *(ABC)*.

https://doi.org/10.55343/CogSust.109

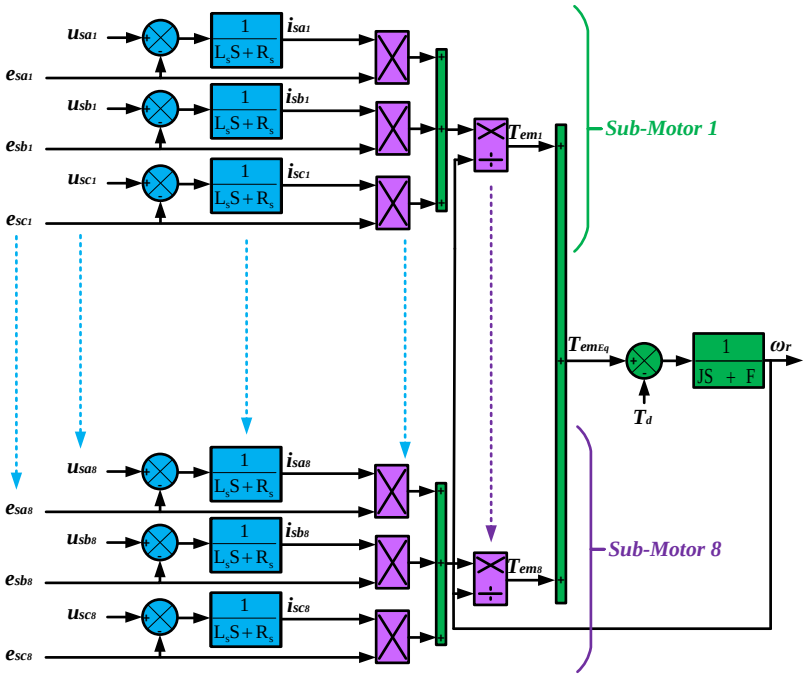

Figure 3. Block diagram of Protean sub-motors in a stationary reference frame *(ABC)*.

3. Protean In-Wheel-Motor Model Given in the Synchronous Reference Frame *(d-q)*

The mathematical model that describes the Protean IWM in the synchronous rotor frame *(d-q)* can be obtained by performing a Park transform from stationary three-axis frame *ABC* into synchronous two-axis frame *d-q* for each sub-motor equation set. First, the three-axis stationary frame *ABC* quantities are projected onto the two-axis stationary frame *α-β* (Clarke transform), which are rotated at the synchronous speed, resulting in orthogonal rotating components *d-q*. Equation (18) presents the Park transform for sub-motor 1.

$$\begin{bmatrix} f_{d_1} \\ f_{q_1} \end{bmatrix} = n_P \begin{bmatrix} \cos(\theta) & \cos(\theta - \frac{2\pi}{3}) & \cos(\theta - \frac{4\pi}{3}) \\ -\sin(\theta) & -\sin(\theta - \frac{2\pi}{3}) & -\sin(\theta - \frac{4\pi}{3}) \end{bmatrix} \begin{bmatrix} f_{A_1} \\ f_{B_1} \\ f_{C_1} \end{bmatrix}, n = 1 \quad (18)$$

The previous matrix can transform the first sub-motor's electrical quantities (voltage, current, and flux) from the three-axis system into the two-axis system. Figure 4 illustrates the Protean sub-motors' phase displacement in stationary *α-β* and synchronous *d-q* reference frames. The Park transform for sub-motor two can be obtained by subtracting the displacement angle of 45° from (18), as follows:

$$\begin{bmatrix} f_{d_2} \\ f_{q_2} \end{bmatrix} = n_P \begin{bmatrix} \cos(\theta - \frac{\pi}{4}) & \cos(\theta - \frac{2\pi}{3} - \frac{\pi}{4}) & \cos(\theta - \frac{4\pi}{3} - \frac{\pi}{4}) \\ -\sin(\theta - \frac{\pi}{4}) & -\sin(\theta - \frac{2\pi}{3} - \frac{\pi}{4}) & -\sin(\theta - \frac{4\pi}{3} - \frac{\pi}{4}) \end{bmatrix} \begin{bmatrix} f_{A_2} \\ f_{B_2} \\ f_{C_2} \end{bmatrix} \quad (19)$$

Similarly, the Park transform for the third sub-motor is obtained by subtracting an angle of 90° according to (20):

$$\begin{bmatrix} f_{d_3} \\ f_{q_3} \end{bmatrix} = n_P \begin{bmatrix} \cos(\theta - \frac{\pi}{2}) & \cos(\theta - \frac{2\pi}{3} - \frac{\pi}{2}) & \cos(\theta - \frac{4\pi}{3} - \frac{\pi}{2}) \\ -\sin(\theta - \frac{\pi}{2}) & -\sin(\theta - \frac{2\pi}{3} - \frac{\pi}{2}) & -\sin(\theta - \frac{4\pi}{3} - \frac{\pi}{2}) \end{bmatrix} \begin{bmatrix} f_{A_3} \\ f_{B_3} \\ f_{C_3} \end{bmatrix} \quad (20)$$

Based on the previous calculations, a general form of the Park transform can be derived for any sub-motor according to (21):

$$\begin{bmatrix} f_{d_n} \\ f_{q_n} \end{bmatrix} = n_P \begin{bmatrix} \cos(\theta - (n-1)\theta_{sm}) & \cos\left(\theta - \frac{2\pi}{3} - (n-1)\theta_{sm}\right) & \cos\left(\theta - \frac{4\pi}{3} - (n-1)\theta_{sm}\right) \\ -\sin(\theta - (n-1)\theta_{sm}) & -\sin\left(\theta - \frac{2\pi}{3} - (n-1)\theta_{sm}\right) & -\sin\left(\theta - \frac{4\pi}{3} - (n-1)\theta_{sm}\right) \end{bmatrix} \begin{bmatrix} f_{A_n} \\ f_{B_n} \\ f_{C_n} \end{bmatrix} \quad (21)$$

https://doi.org/10.55343/CogSust.109

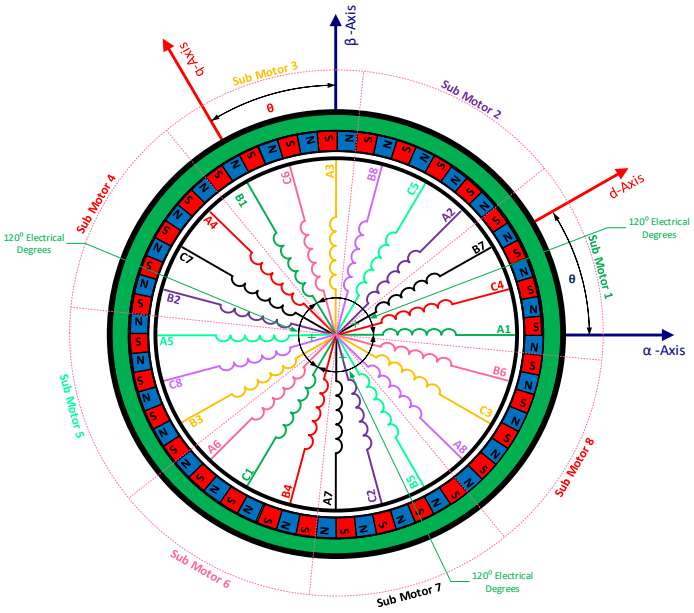

Figure 4. A Protean sub-motors' phase displacement in stationary *α-β* and synchronous *d-q* reference frames, respectively.

where:

f_{d_n}, f_{q_n}: direct and quadrature magnetic and electrical quantities for any sub-motor *(n)* in synchronous reference frame *d-q*.

$f_{A_n}, f_{B_n}, f_{C_n}$: three-phase magnetic and electrical quantities for any sub-motor *(n)* in stationary reference frame *ABC*.

n_P: the Park transform constant, which has two values: $n_P = \frac{2}{3}$ for transforming while maintaining fixed magnitudes (to be adopted in this research) and $n_P = \sqrt{\frac{2}{3}}$ for transforming while maintaining fixed powers.

Each sub-motor in the Protean motor can be considered an independent permanent magnet motor, considering that in the surface-mounted permanent magnets (SPM) motor, the *d-q* inductances are equal ($L_d = L_q$). Thus, stator voltages and fluxes of any sub-motor *(n)* are given in the *d-q* synchronous reference frame as follows:

$$L_d \frac{di_{d_n}}{dt} = -R_s i_{d_n} + P\omega_r L_q i_{q_n} + u_{d_n} \quad (22)$$

$$L_q \frac{di_{q_n}}{dt} = -R_s i_{q_n} - P\omega_r L_d i_{d_n} - P\omega_r \varphi_f + u_{q_n} \quad (23)$$

$$\varphi_{d_n} = l_d i_{a_n} + \varphi_f \quad (24)$$

$$\varphi_{q_n} = l_q i_{q_n} \quad (25)$$

The electromagnetic torque resulting from each sub-motor in the Protean motor is expressed in terms of the orthogonal interaction of the flux and current components according to the following equation:

$$T_{em_n} = \frac{3}{2} P\left(\varphi_{d_n} i_{q_n} - \varphi_{q_n} i_{d_n}\right) \quad (26)$$

Considering that each sub-motor will be controlled to provide the maximum torque per ampere (MTPA) with $i_{q_n} = I_{s_n}$ and $i_{d_n} = 0$, the electromagnetic torque equation for any sub-motor *(n)* can be rewritten as follows:

$$T_{em_n} = \frac{3}{2} P\left(\varphi_f i_{q_n}\right) \quad (27)$$

The previous equation is also applicable for controlling the motor to achieve speeds beyond base speed through field weakening (FW), where the inductance torque component is negligible due to the inductance equality: $(L_{sd} - L_{sq}) i_{d_n} i_{q_n} = 0$ in the SPM motor. As for the total torque of a Protean motor, it is the sum of all sub-motors torques according to:

$$T_{em_{Eq}} = \sum_{n=1}^{8} T_{em_n} \quad (28)$$

https://doi.org/10.55343/CogSust.109

Equivalently, torque can be expressed in terms of the orthogonal interaction current and flux of all sub-motors as follows:

$$T_{em_{Eq}} = \frac{3}{2} P \left(\varphi_{d_{Eq}} i_{q_{Eq}} - \varphi_{q_{Eq}} i_{d_{Eq}} \right) \quad (29)$$

where:

$$i_{d_{Eq}} = \sum_{n=1}^{8} i_{d_n} \quad (30)$$

$$i_{q_{Eq}} = \sum_{n=1}^{8} i_{q_n} \quad (31)$$

$$\varphi_{d_{Eq}} = \sum_{n=1}^{8} \varphi_{d_n} \quad (32)$$

$$\varphi_{q_{Eq}} = \sum_{n=1}^{8} \varphi_{q_n} \quad (33)$$

As for the speed of the common rotor is given in the equation (34):

$$J_r \frac{d\omega_r}{dt} = T_{em_{Eq}} - T_L \quad (34)$$

The rotor position can be obtained by integrating the mechanical speed according to (35):

$$\theta_r = \int \omega_r \, dt \quad (35)$$

where:

u_{d_n}, u_{q_n}: direct and quadrature voltage components of sub-motor (n) in the synchronous reference frame *d-q*.

i_{d_n}, i_{q_n}: direct and quadrature current components of sub-motor *(n)* in the synchronous reference frame *d-q*.

I_{s_n}: current vector of sub-motor *(n)*.

L_d, L_q: direct and quadrature inductance components for sub-motor *(n)* in the synchronous reference frame *d-q*.

$\varphi_{d_n}, \varphi_{q_n}$: direct and quadrature flux components for sub-motor *(n)* in the synchronous reference frame *d-q*.

$i_{d_{Eq}}, i_{q_{Eq}}$: equivalent direct and quadrature current components for all sub-motors in the synchronous reference frame *d-q*.

$\varphi_{d_{Eq}}, \varphi_{q_{Eq}}$: equivalent direct and quadrature flux components for all sub-motors in the synchronous reference frame *d-q*.

$T_{em_n}, T_{em_{Eq}}$: torque and equivalent torque for one sub-motor *(n)* and all sub-motors, respectively.

φ_f: permanent magnet's flux.

Figure 5 illustrates the complete block diagram of the Protean motor represented in the synchronous reference frame *d-q*. This is presented by displaying the first and last sub-motors (where the other sub-motors have the same model). The upper section illustrates the current model. As for the flux and electromagnetic torque model, it is shown in the lower section. The total torque for the Protean motor is the torque sum of all sub-motors, where the torque balance of the total torque and the load torque is the input to the common rotor of the Protean motor.

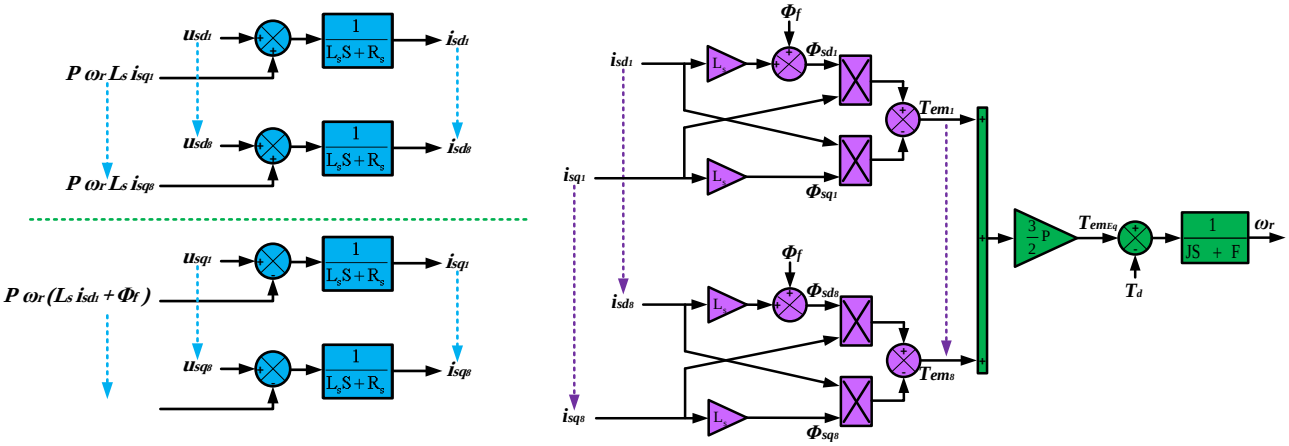

Figure 5. A block diagram of the Protean sub-motors is represented in the synchronous reference frame *d-q*.

4. Simulation Results

To validate the Protean IWM mathematical model, simulation models for the motor and its vector control were built in MATLAB/Simulink. The control is designed to run the motor primarily in the MTPA mode at speeds below the base speed (1000 rpm). Upon exceeding this speed, it automatically switches to FW mode using the state flow logic in MATLAB. To

https://doi.org/10.55343/CogSust.109

validate the independent control of sub-motors, MTPA mode is activated first, followed by FW mode running when a higher speed is requested.

Figure 6 illustrates the motor speed response to a gradual speed request. Initially, a reference speed corresponding to the base speed of 1000 rpm is requested, representing an operation in the constant torque region (CTR). The time to reach the desired speed is 0.7 seconds, and at second 1, the motor is loaded with the nominal load, causing a slight decrease in speed, as shown in the magnified portion. The controller quickly compensates for this decrease, restoring the motor speed. Working under MTPA mode continues until second 2 when the system switches to the constant power region (CPR) through the FW. The required speed in this case corresponds to maximum speed at 1400 rpm, where this condition lasts until the end of the simulation at second 3.5.

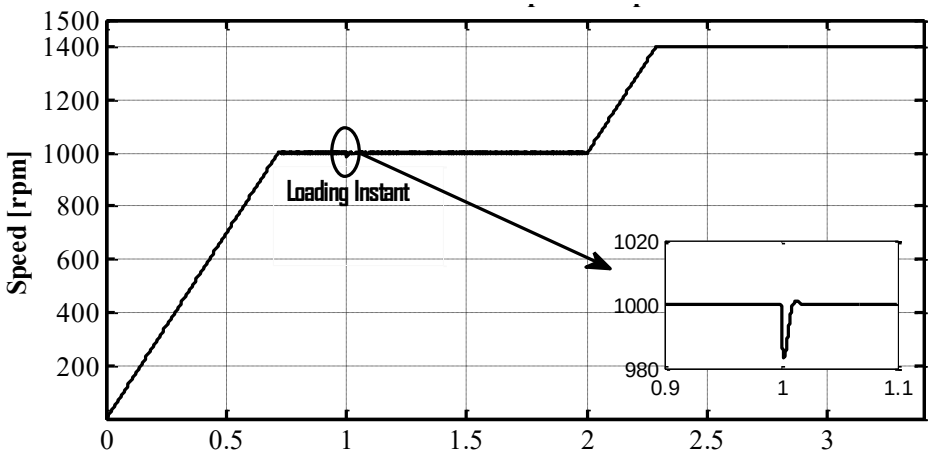

Figure 6. Protean IWM speed response under CTR-MTPA and CPR-FW control modes.

Figure 7 shows the Protean motor response to a working point with nominal torque at a speed of 1000 rpm. It is noted that the motor was able to develop the full torque of 500 Nm, which is the continuous operating torque indicating the validation of the motor model. When operating in the CPR region, we observe a decrease in the developed torque to approximately 370 Nm due to the position change of the current vector of each sub-motor I_{s_n} in response to field weakening.

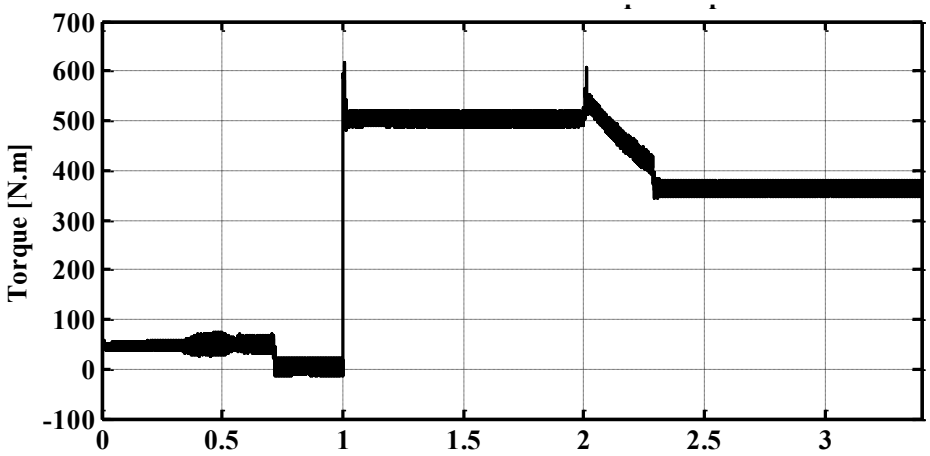

Figure 7. Protean IWM torque response under CTR-MTPA and CPR-FW control modes.

5. Conclusion

This paper presents and studies a new type of advanced IWM system designed by Protean Electric. The Protean IWM system is considered a highly integrated system with high torque density and high fault tolerance. Fault tolerance is ensured by dividing the stator into eight independent sub-motors with a common rotor. Each of the eight sub-motors constitutes a completely independent unit with its drive system and integrated micro-inverter. This motor has a high continuous torque of

https://doi.org/10.55343/CogSust.109

up to 500 Nm and a maximum torque of up to 1000 Nm. The mathematical model of this motor is derived based on a set of Park transforms corresponding to each sub-motor's spatial and electrical distribution.

A Protean motor system was developed in the MATLAB/Simulink environment to validate the mathematical model derivation, allowing independent control of each sub-motor. The simulation results show the correctness of mathematical model derivation by applying vector control independently to each sub-motor.

Abbreviations

ABS	Anti-lock braking System
ACAS	Advanced Chassis Active-Safety Systems
BBW	Brake-by-Wire
EV	Electric Vehicle
EWB	Electronic Wedge Brake
FW	Flux Weakening
IWM	In-Wheel-Motor
MTPA	Maximum Torque per Ampere
PMSM	Permanent Magnet Synchronous Motor
RABS	Regenerative Anti-lock braking System
SPM	Surface-Mounted Permanent Magnet
TCS	Traction Control System
TV	Torque Vectoring

References

Deepak, K., Frikha, M. A., Benômar, Y., El Baghdadi, M., Hegazy, O. (2023). In-Wheel Motor Drive Systems for Electric Vehicles: State of the Art, Challenges, and Future Trends. *Energies*. 16(7), 1–31. DOI: 10.3390/en16073121

Feng, Z., Zhao, S., Gao, W., Zhang, Y., Fei, L. (2023). Study on a Novel In-Wheel Motor Driving System Driven by Two Permanent Magnet Synchronous Disc Motors. *IEEE Transactions on Vehicular Technology*. 72(5), 5922–5933. DOI: 10.1109/TVT.2023.3233997

Fraser, A. (2018). *In-Wheel Electric Motors – The Packaging and Integration Challenges*. Protean Electric. URL: https://www.proteanelectric.com/f/2018/04/In_Wheel_Electric_Motors_AFraser_ProteanV4.pdf.

Hilton, C. (2016) *Wheel Torque and Speed in a Vehicle with In-Wheel Motors*. Protean Electric. URL: https://www.proteanelectric.com/f/2018/04/Wheel_Torque_and_Speed_in_a_Vehicle_with_In-Wheel_Motors.pdf

Ifedi, C. J., Mecrow, B. C., Brockway, S. T. M., Boast, G. S., Atkinson, G. J., Kostic-Perovic, D. (2011). Fault tolerant in-wheel motor topologies for high performance electric vehicles. *2011 IEEE International Electric Machines and Drives Conference, IEMDC 2011*. 1310–1315. DOI: 10.1109/IEMDC.2011.5994794

Ifedi, C. J., Mecrow, B. C., Widmer, J. D., Atkinson, G. J., Brockway, S. T. M., Kostic-Perovic, D (2012). A high torque density, direct drive in-wheel motor for electric vehicles. *IET Conference Publications*, 2012(592 CP). DOI: 10.1049/cp.2012.0254

Perovic, D. K. (2012). Making the impossible, possible-overcoming the design challenges of in wheel motors. *World Electric Vehicle Journal*. 5(2), 514–519. DOI: 10.3390/wevj5020514

Said Jneid, M. (2024). Radial Flux In-Wheel-Motors for Vehicle Electrification. *Cognitive Sustainability*. 3(3). DOI: 10.55343/cogsust.105

Said Jneid, M., Harth, P. (2023a). Blended Regenerative Anti-Lock Braking System and Electronic Wedge Brake Coordinate Control Ensuring Maximal Energy Recovery and Stability of All-Wheel-Motor-Drive Electric Vehicles. *Journal of Transportation Technologies*. 13(03), 465–495. DOI: 10.4236/jtts.2023.133022

Said Jneid, M., Harth, P. (2023b). Coordinate Torque Vectoring Control For Enhancing Handling and Stability of All-Wheel-Drive Electric Vehicles Through Wheel Slip Control Integration. *2023 IEEE Cognitive Mobility Conference (CogMob)*. 177–186. Budapest, Hungary: IEEE.

Said Jneid, M., Harth, P. (2023c). Integrated Braking and Traction Torque Vectoring Control Based on Vehicle Yaw Rate for Stability Improvement of All-Wheel-Drive Electric Vehicles. *2023 IEEE International Conference on Electrical Systems for Aircraft, Railway, Ship Propulsion and Road Vehicles & International Transportation Electrification Conference (ESARS-ITEC)*. 1–6. Venice, Italy: IEEE. DOI: 10.1109/ESARS-ITEC57127.2023.10114899

Said Jneid, M., Harth, P. (2023d). Integrated Torque Vectoring Control Using Vehicle Yaw Rate and Sideslip Angle for Improving Steering and Stability of All Off-Wheel-Motor Drive Electric Vehicles, *Acta Polytechnica Hungarica*. 21(7), 87–106. DOI: 10.12700/APH.21.7.2024.7.6

Said Jneid, M., Joukhadar, A. (2019). LQR-Based Control of a Single Motor Electronic Wedge Brake EWB for Automotive Brake-By-Wire System. *Soft Computing and Electrical Engineering*. 1(1), 12–35. URL: https://paper.ieti.net/scee/2019Volume1Issue1/paper02.pdf

Said Jneid, M., Harth, P., Ficzere, P. (2020). In-Wheel-Motor Electric Vehicles And Their Associated Drivetrains. *International Journal For Traffic And Transport Engineering*. 10(4). DOI: 10.7708/ijtte.2020.10(4).01

Said Jneid, M., Zöldy, M., Harth, P. (2023). Sensorless optimal control of electronic wedge brake based on dynamic model and Kalman filter state multiple-estimation. *Proceedings of the Institution of Mechanical Engineers, Part D: Journal of Automobile Engineering*. 238(1): 095440702311681. DOI: 10.1177/09544070231168168

Whitehead, A., Hilton, C. (2018). Protean Electrics In-Wheel Motors Could Make EVs More Efficient. *IEEE Spectrum*. 1–10.